Reconstructing seafloor bathymetry with a multichannel broadband InSAS using Belief Propagation

P. J. Barclay, C. J. Forne, M. P. Hayes, and P. T. Gough

Acoustics Research Group,
Dept. of Electrical and Computer Engineering,
University of Canterbury,
Private Bag 4800, Christchurch, New Zealand

{*p.barclay,c.forne,m.hayes,p.gough*}*@elec.canterbury.ac.nz*

***Abstract*— Synthetic Aperture Sonar (SAS) provides high resolution imagery with range independent resolution. However, imagery has been limited to two-dimensions, showing acoustic reflectivity for a given scene. To further enhance the usefulness of a SAS system this needs to be combined with a topographical height map of the same scene. This paper presents a novel technique to obtain the third-dimension by first remapping on to a set of common ground-planes, with the most likely surface through this volume found using Belief Propagation. This technique allows any a priori information to be incorporated and thus provides a maximum a posteriori (MAP) estimate of the seafloor height. Results are presented from a rough seafloor simulator with height reconstructions using this technique.**

I. Introduction

Synthetic aperture sonar (SAS) is similar to synthetic aperture radar (SAR) in that it can generate high-resolution imagery independent of range. This is achieved through coherent summation of successive echo signals to synthesise an aperture many times longer than the towfish [1]. While the synthetic aperture technique generates high-resolution imagery, it does not provide bathymetric information regarding the topology of the seafloor. A solution to this is to use two or more vertically separated receivers. By measuring the delay differences between the displaced receivers, the angle of arrival of the incident echo wavefront can be estimated. Then combining the angle estimates with the range measurements, an estimate of the height of the scatterers can be derived.

While interferometric aperture synthesis has been successfully achieved in radar (InSAR) [2]–[4], the sonar equivalent is complicated by the slow speed of sound necessitating wider beamwidths and broader bandwidths, by unwanted reflections from the sea-surface, and by greater unknown motion errors.

The technique presented in this paper employs a statistical filtering approach to search a volume of height likelihoods. This volume is generated by remapping the slant-range imagery onto a set of height differing ground-planes. The approach eliminates the need for 2-D phase unwrapping required by direct interferometry techniques.

The imagery presented in Sec. (IV) is obtained from simulations of the KiwiSAS-IV system developed at the University of Canterbury. This sonar system operates simultaneously at two frequency bands centered on 30 kHz and 100 kHz, each with a bandwidth of 20 kHz. The system has one projector, and three vertically separated hydrophones simultaneously sampled. For more details of this system see [5], [6].

II. Direct Interferometry

An interferogram is formed from two complex images (q_1), and (q_2) by taking the Hermitian product of the two complex images

$$\chi = q_1 q_2^* \tag{1}$$

where $(^*)$ denotes the complex conjugate. The interferogram is then simply the phase of χ

$$\hat{\psi} = \angle \chi \tag{2}$$

The interferometric phase can then be used to estimate the height of the imaged slant range point. This can be calculated for every point in the images, resulting in an overall three-dimensional topography estimate. This technique is well established in both airborne and spaceborne Synthetic Aperture Radar (SAR) systems [3], and more recently Synthetic Aperture Sonar (SAS) [7]–[10].

Due to the specular nature of SAS imagery, any shift in imaging geometry causes a decorrelation [11]. Since interferometry uses two different imaging looks of the scene, decorrelation effects can be observed. This has the effect of producing speckly interferograms, with largely altered phase differences for a small change in imaging geometry. If these phase differences are used directly to produce a height estimate of the original scatterer, unreasonable height variations can occur.

The interferometric phase difference is also calculated modulo (2π) requiring two-dimensional phase unwrapping [12] in all but a few special interferometric applications [13].

0-933957-31-9

III. Bayesian Height Estimation

Some SAR researches have measured the coherence between pairs of ground-plane remapped data to estimate the correct depth [3]. However for shallow water SAS the coherence only varies slightly with seafloor depth error resulting in low height resolution.

In this paper we estimate the seafloor height be remapping the data over many different heights to create a volume of hydrophone variances. This volume is then searched for a minimum to give a seafloor surface estimate. This approach works with an arbitrary number of hydrophones and frequency bands and is a maximum likelihood (ML) estimator. However due to residual decorrelations in the data, the height estimates are noisy so we then statistically filter these estimates including a prior information about the expected seafloor topography. This then provides a maximum a posteriori (MAP) estimate of the seafloor height.

This process can be divided into four steps:

1) Generate volume of ground-plane remapped images.
2) Calculate variance of each voxel.
3) Convert voxel variance to likelihoods.
4) Find MAP estimate of height using Belief Propagation.

A. Groundplane Remapping

During the Synthetic Aperture reconstruction process the third dimension (height) of the scene is not used. Instead the height is assumed to be zero, and all reconstruction is done on the slant-range plane. This has the effect of producing an increasing acrosstrack shift in the image for increasing height difference between the sonar and the seafloor. For an interferometric setup, the hydrophones are vertically separated but all share a common transmitter array. Thus the acoustic path difference is dominated by the acoustic receive path only.

To compensate for the differing receiver path lengths, groundplane remapping can be performed to resample the data from the various slant range planes to a common groundplane. To do this remapping the topography of the seafloor must be known. Since this height information is not known initially an estimate must be made. From this initial height estimate the true distance to a given acrosstrack point can be found, then used as an index into the original slant range plane data. Subsample interpolation must then be used to estimate the signal at the corrected range. A phase correction term is also applied corresponding to the phase change of the original modulated signal.

For each receiver R_n the geometry is as shown in Fig. 1 where s is the slant-range data, and g the remapped ground-plane data. The envelope remapping is then given by the equations:

$$\begin{aligned} s_n(x) &= \sqrt{g(x)^2 + (g(z) - R_n(z))^2} \\ s_n(y) &= g(y) \end{aligned} \tag{3}$$

The phase correction term required to compensate for the demodulation of the original acoustic signal is then

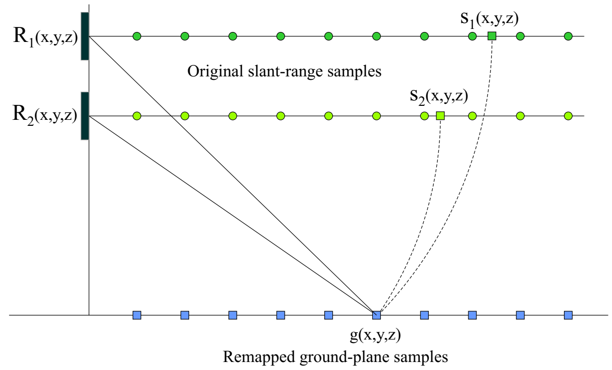

Fig. 1. Remapping slant-range plane to ground-plane.

$$\varphi = \exp\left(\frac{-j4\pi f_c s(x)}{c}\right) \tag{4}$$

where f_c is the center frequency, (c) is the speed of sound in water.

The overall effect of this process can be seen in Fig.2, for the case of a single point reflector located 45 m directly acrosstrack, 5 m below the sonar. Notice the peaks of the original slant range curves are centered at approximately 45.2 m, and after remapping to the correct groundplane they are centered on the original simulation position of 45 m.

For a flat seafloor scene, ground-plane remapping can be seen by comparing the interferograms of the original slant-range plane data, and after remapping to the 'correct' ground-plane as shown in Fig.3. The original interferogram is very speckly in nature, and shows several interference fringes in range across the image. After remapping to the 'correct' height-plane the speckle has been reduced, and the interference fringes have been removed leaving a mean phase difference of zero. The speckle reduction is as a result of decreasing the decorrelation between the scenes with corresponding pixels footprints now aligned. The remaining speckle is from the slightly different angle of viewing of the scene from the two receivers [14]. Bands of higher speckle can be seen across the interferogram at ranges of 23 m, 11 m, 6 m, and several < 5 m corresponding to the nulls in the vertical beam pattern of the transducers.

B. Calculating Variance

The variance between the remapped images is calculated using

$$v = \sum \frac{|\hat{q}_n - \mu|^2}{n-1} \tag{5}$$

where μ is the mean of $\hat{q}_n$ and n is the number of receivers.

C. Conversion to Likelihoods

Each remapped pixel on each ground-plane is converted to a likelihood. This likelihood gives a measure of how likely the pixel has been correctly remapped. To do this the samples are assumed to be from a normal distribution, so the likelihood L

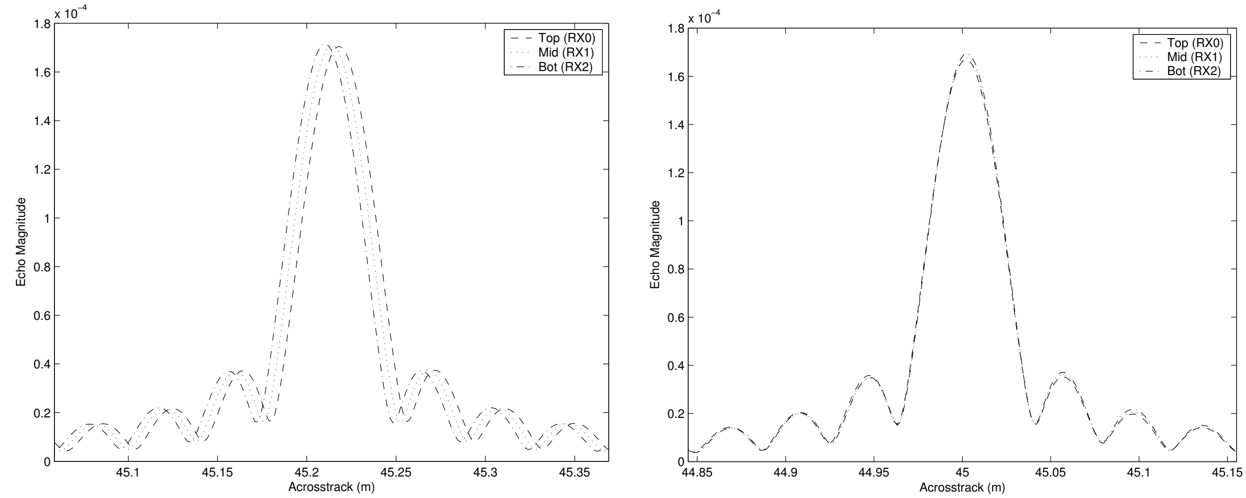

(a) (b)

Fig. 2. Signal envelope of a single point target at 40 m range, 5 m below sonar. (a) reconstructed on slant range plane, and (b) remapped to correct groundplane.

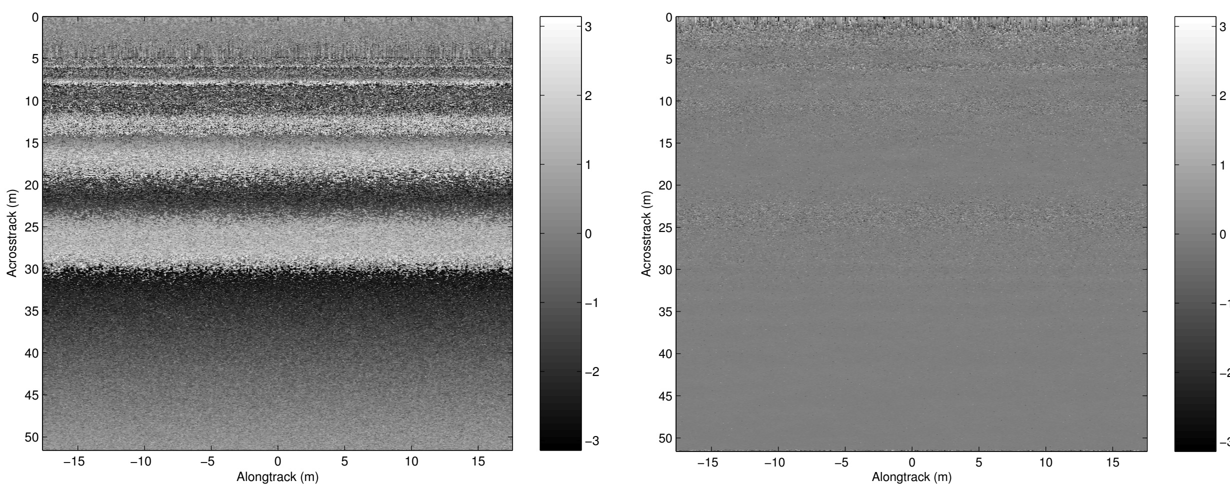

(a) (b)

Fig. 3. Interferogram for (a) slant-range plane data, and (b) ground-plane data remapped to the 'correct' height. Receiver separation 0.15 m.

at pixel i for the h^{th} height can be derived from the variance v of the complex samples using

$$L = \frac{1}{\sqrt{2\pi a}} \exp\left(-\frac{v^2}{2a^2}\right) \tag{6}$$

where a is the variance of the distribution. This relationship relies on the remapped vectors having low variance when remapped onto the correct ground-plane. An initial height map can be obtained from this likelihood volume by taking the maximum likelihood for each pixel.

D. Belief Propagation

Belief Propagation is an efficient technique based on local message passing can be used to find the most likely state of a system given any available evidence. By appropriately modeling the system, this approach can be applied to bathymetric data to produce an improved estimate the sea floor. Although originally proposed by Pearl [15] for performing probabilistic reasoning on Bayesian networks, the technique and has since been successfully applied to the stereo imaging field [16]–[18]. In most of this work, the system is modeled as a hidden Markov Random Field (MRF). Belief Propagation is then applied to this model, acting as a statistical filter to find the most likely surface, given a volume of measured likelihood estimates and the expected variation between neighbouring points.

To apply this technique to bathymetric data, the scene is represented as a connected 2D array of nodes, whose value corresponds to surface height. Associated with each node are a set of beliefs which give a measure how likely the surface is to be at any particular height. The objective is to calculate these beliefs as accurately as possible, by propagating the original data throughout the network.

Using the "max-product" algorithm [19], the belief B at a node i for the h^{th} height at the n^{th} iteration is computed using

$$B_i^n(h) = L_i(h) \prod_{j \in N(i)} M_{ji}^n(h), \tag{7}$$

where $N(i)$ is the set of neighbouring nodes to node i, $L_i(h)$ is the initial likelihood computed from the measurement data, and where $M_{ji}^n(h)$ is the message from node j to node i at iteration n, computed by

$$M_{ji}^n(h) = \max_{h'} \left(\Psi(h, h') \frac{B_j^n(h')}{M_{ij}^{n-1}(h')} \right). \tag{8}$$

Here $\Psi(h, h')$ is a compatibility function that describes the joint probability distribution of neighbouring node heights, and $M_{ij}^{n-1}(h)$ is the message from node i to node j from the previous iteration.

In practice the messages are normalised, and a time average operation is performed to stabilise the algorithm and prevent local oscillations

$$M_{ij}^n(h) = \frac{M_{ij}^{n-1}(h) + M_{ij}^n(h)}{\sum_{h=1}^{H} \left(M_{ij}^{n-1}(h) + M_{ij}^n(h) \right)} \tag{9}$$

where H is the number of height measurements and the initial messages are given an identical weighting,

$$M_{ji}^0(h) = H^{-1}. \tag{10}$$

The algorithm runs iteratively until it converges to a steady solution after approximately 40 iterations. The most likely surface is given by the height at each node with the highest belief value. In other words,

$$\hat{h}_i = \max_h B_i(h). \tag{11}$$

IV. Imagery

The simulations are of a rough seafloor using a Monte Carlo integration of many simple point scatterer responses. This model neglects occlusion and multiple scattering but gives a reasonable approximation of the coherent speckle effects that occur with a real sonar. The rough seafloor was modeled as a fractal surface with a Goff-Jordan power spectrum [20] using an approximate Fourier method with oversampling. The 'man-made' objects are then introduced by modifying the reflector heights using an analytical terrain description.

Fig. 5 shows an example of groundplane remapping and height reconstruction using belief propagation. The scene is based on a rough seafloor with a mean depth of 10 m. The scene also contains a large 'crater'.

V. Conclusion

Through application of the Belief Propagation algorithm to SAS imagery a three-dimensional topography of the seafloor can be obtained. This algorithm searches through a likelihood volume locating the most likely surface given a priori information regarding the likelihood of a height change between neighbouring pixels. This surface at each pixel is limited in height to that of the chosen remapped ground-planes. This produces a quantised height map resulting in large height steps and therefore height errors of up to one quantisation step. To reduce this error the algorithm need to be extended to allow for a continuous height variable at each pixel.

VI. Acknowledgments

Philip Barclay would like to thank the University of Canterbury for his Doctoral Scholarship. Chris Forne would like to thank the New Zealand Foundation for Research, Science Technology for his top achiever Doctoral Scholarship.

References

[1] D. W. Hawkins and P. T. Gough, "Imaging algorithms for a strip-map synthetic aperture sonar: minimizing the effects of aperture errors and aperture undersampling," *IEEE J. Oceanic Engineering*, vol. 22, no. 1, pp. 27–39, January 1997.

[2] F. Gatelli, A. M. Guarnieri, F. Parizzi, P. Pasquali, C. Prati, and F. Rocca, "The wavenumber shift in SAR interferometry," *IEEE Transactions on Geoscience and Remote Sensing*, vol. 32, no. 7, pp. 855–865, July 1994.

[3] L. M. H. Ulander and P. Frölind, "Ultra-wideband SAR interferometry," *IEEE Trans. Geoscience and Remote Sensing*, vol. 36, no. 5, pp. 1540–1550, September 1998.

[4] J. Homer, I. D. Longstaff, Z. She, and D. Gray, "High resolution 3-D imaging via multi-pass SAR," *IEE Proc. Radar, Sonar, and Navigation*, vol. 149, no. 1, pp. 45–50, February 2002.

[5] P. J. Barclay, M. P. Hayes, and P. T. Gough, "Multi-channel data acquisition for a free-towed synthetic aperture sonar," in *Proceedings of Electronics New Zealand Conference*, Dunedin, New Zealand, November 2002, pp. 133–138.

[6] M. P. Hayes, P. J. Barclay, and T. J. Hawkins, "An embedded compact PCI computer system for a synthetic aperture sonar towfish," in *Proceedings of Electronics New Zealand Conference*, Dunedin, New Zealand, November 2002, pp. 139–144.

[7] S. M. Banks, H. D. Griffiths, and T. J. Sutton, "A technique for interferometric synthetic aperture sonar image processing," in *London Communications Symposium*, September 2001.

[8] P. J. Barclay, M. P. Hayes, and P. T. Gough, "Using a multi-frequency synthetic aperture sonar for bathymetry," in *Image and Vision Computing New Zealand 2001*, University of Otago, Dunedin, New Zealand, November 2001, pp. 63–68.

[9] W. W. J. Bonifant, M. A. Richards, and J. H. McClellan, "Interferometric height estimation of the seafloor via synthetic aperture sonar in the presence of motion errors," in *IEE Proceedings - Radar, Sonar and Navigation*, vol. 147, no. 2. IEE, December 2000, pp. 322–330.

[10] L. Wang, A. Bellettini, R. Hollett, A. Tesei, and M. Pinto, "InSAS'00: Interferometric SAS and INS aided SAS imaging," in *Oceans 2001*, vol. 1. IEEE, November 2001, pp. 179–187.

[11] J. C. Dainty, Ed., *Laser Speckle and Related Phenomena*, ser. Topics in Applied Physics. Springer-Verlag, 1975, vol. 9.

[12] R. M. Goldstein, H. A. Zebker, and C. L. Werner, "Satellite radar interferometry: Two-dimensional phase unwrapping," *Radio Science*, vol. 23, no. 4, pp. 713–720, July-August 1988.

[13] D. Massonnett, H. Vadon, and M. Rossi, "Reduction of the need for phase unwrapping in radar interferometry," *IEEE Trans. Geosci. Remote Sensing*, vol. 34, pp. 489–497, May 1996.

[14] A. J. Hunter, M. P. Hayes, and P. T. Gough, "Simulation of wideband interferometric SAS imagery," in *Oceans 2003*, September 2003.

[15] J. Pearl, *Probabilistic reasoning in intelligent systems: networks of plausible inference*, 2nd ed. Morgan Kaufmann Publishers, San Mateo, Calif., 1988.

[16] J. Sun, H. Y. Shum, and N. N. Zheng, "Stereo matching using belief propagation," in *Proceedings of the European Conference on Computer Vision*, vol. 2, Copenhagen, Denmark, May 2002, pp. 510–524.

[17] N. Petrovic, I. Cohen, B. J. Frey, R. Koetter, and T. S. Huang, "Enforcing integrability for surface reconstruction algorithms using belief propagation in graphical models," in *Computer Vision and Pattern Recognition, 2001*, vol. 1. IEEE, 2001, pp. I–743 – I–748.

[18] A. Minagawa, K. Uda, and N. Tagawa, "Region bxtraction based on belief propagation for gaussian model," in *Pattern Recognition, 2002 Proceedings*, vol. 2. IEEE, 2002, pp. 507–510.

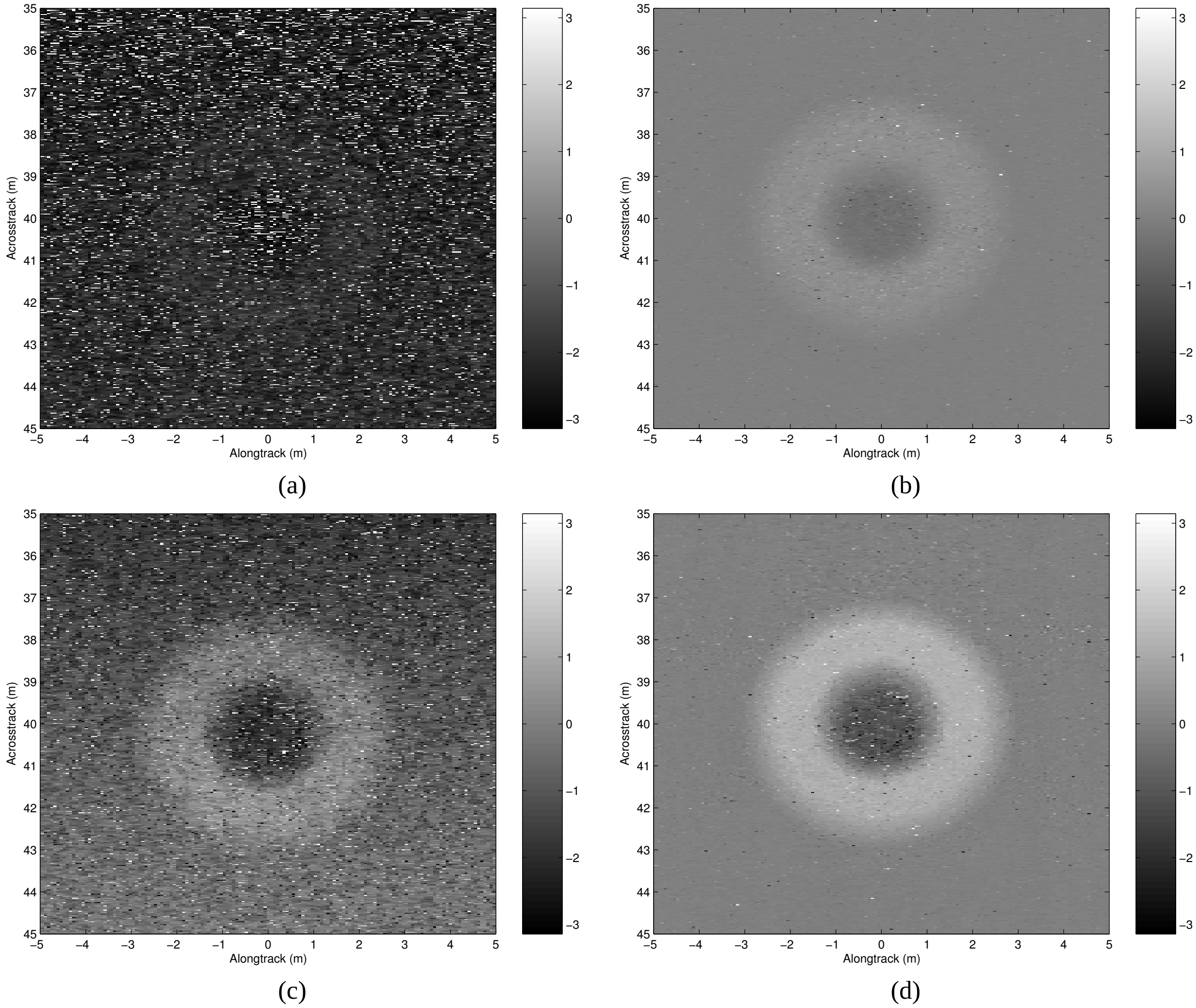

Fig. 4. Interferograms of a smaller crater of height 0.75 m on a seafloor of 10 m mean depth. (a) Slant range plane interferogram ($f_c = 30\,kHz$). (b) Remapped to estimated groundplane interferogram ($f_c = 30\,kHz$). (c) Slant range plane interferogram ($f_c = 100\,kHz$). (d) Remapped to estimated groundplane interferogram ($f_c = 100\,kHz$).

[19] Y. Weiss and W. T. Freeman, "On the optimality of solutions of the max-product belief-propagation algorithm in arbitrary graphs," *IEEE Trans. Inform. Theory*, vol. 47, no. 2, pp. 735–744, February 2001.

[20] J. A. Goff and T. H. Jordan, "Stochastic modeling of seafloor morphology: Inversion of sea beam data for second-order statistics," *Journal of Geophysical Research*, vol. 93, no. B11, pp. 13 589–13 608, November 1988.

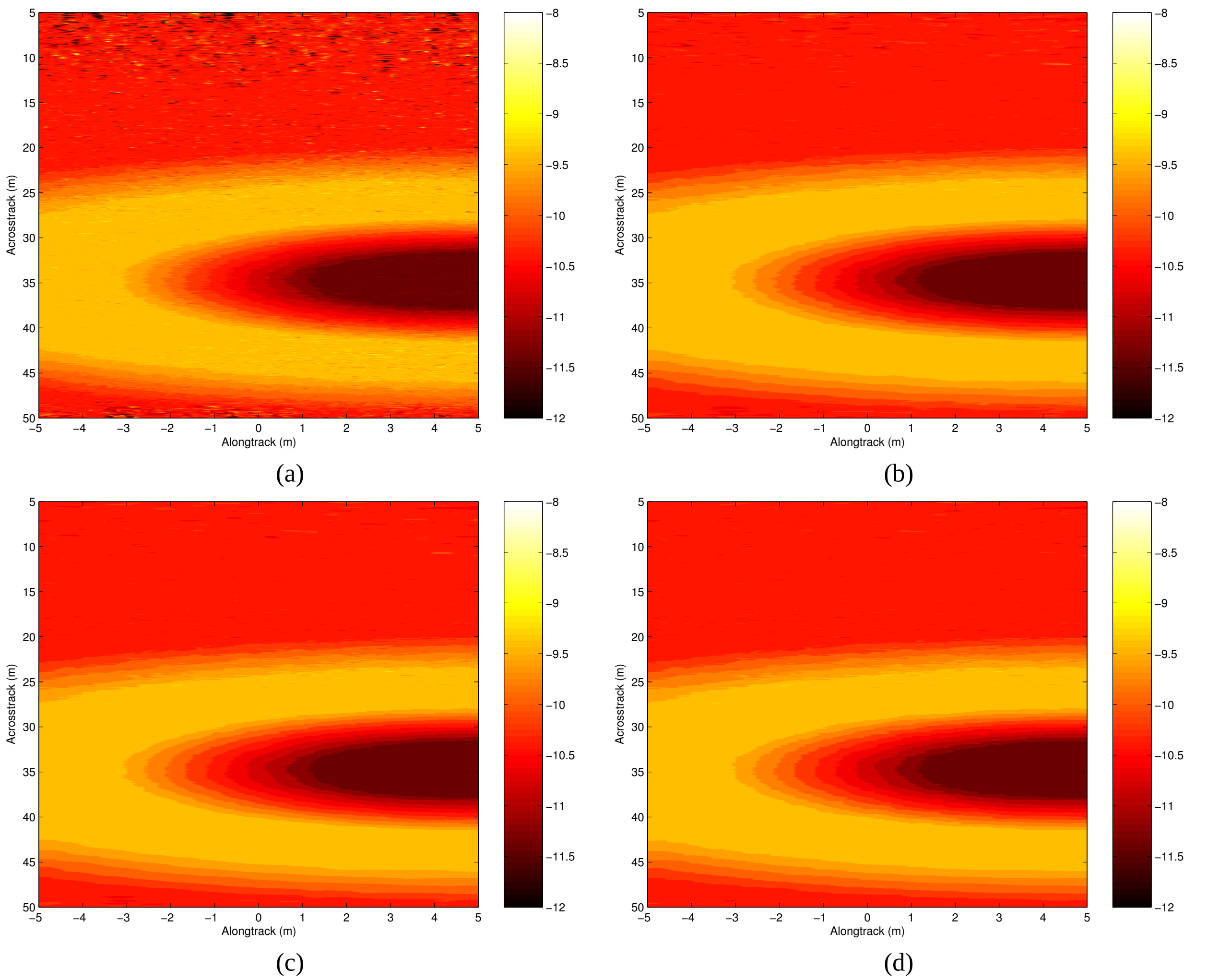

Fig. 5. Height reconstruction using Belief Propagation for a larger 'crater' of height 1 m with center -1 m on a rough seafloor of mean depth 10 m. (a) 1 iteration. (b) 5 iterations. (c) 10 iterations. (d) 20 iterations.